

# Tensile and compressive properties of AISI 304L stainless steel subjected to equal channel angular pressing

S. Qu<sup>a</sup>, C.X. Huang<sup>a</sup>, Y.L. Gao<sup>b</sup>, G. Yang<sup>b</sup>, S.D. Wu<sup>a,\*</sup>, Q.S. Zang<sup>a</sup>, Z.F. Zhang<sup>a,\*</sup>

<sup>a</sup> Shenyang National Laboratory for Materials Science, Institute of Metal Research, Chinese Academy of Science, Shenyang 110016, China

<sup>b</sup> Central Iron and Steel Research Institute of Beijing, 100081 Beijing, China

Received 25 January 2007; received in revised form 9 April 2007; accepted 27 April 2007

## Abstract

The present work investigated the compressive and tensile properties of AISI 304L austenitic stainless steel subjected to equal channel angular pressing (ECAP) at high temperature (700 °C). Tensile and compressive strength, elongation, Vickers hardness and fracture mode of annealed and ECAPed material were systematically compared. It is found that with increasing the number of ECAP passes the tensile strength and hardness increase, however, the elongation and strain hardening rate decrease. The compressive yield strength and strain hardening rate displayed obvious anisotropy when the ECAPed austenitic stainless steel was compressed along different orientations. The tensile fracture mode was changed from the ductile to brittle feature with increasing the number of ECAP passes. Accordingly, the ECAPed steel exhibited apparent asymmetry in tensile and compressive properties. Besides, the relationship between strength and Vickers hardness was established. Based on the results above, the corresponding deformation and fracture mechanisms were discussed.

© 2007 Published by Elsevier B.V.

**Keywords:** AISI 304L stainless steel; Equal channel angular pressing (ECAP); Compression; Tension; Mechanical properties; Fracture modes

## 1. Introduction

Equal channel angular pressing (ECAP) is presently one of the most promising techniques which can produce ultra-fine grained (UFG) materials (grain size in the range of 10–1000 nm) through the process of simple shear by pressing a sample through a die with two intersecting channels, equal in cross-section [1–4]. The sample is simply pressed through the channel and a shear strain is introduced to the sample when it passes through the bending point of the channel [5]. Repetitive pressing is feasible as the sample cross-section remains unchanged. A high total strain is then achieved during a process of multiple-pass pressing [6]. Between each successive pressing, it is possible to select one of the four distinct routes, designated as routes A, B<sub>A</sub>, B<sub>C</sub> and C, respectively, in which the sample is rotated 0°, 90° and 180° along its longitudinal axis, respectively. However, the routes designated as routes B<sub>A</sub> and B<sub>C</sub> refer to a rotation of 90° in the opposite sense and in the same sense between consec-

utive passes, respectively [7]. The four processing routes were examined earlier with reference to the macroscopic distortions occurring on the X, Y and Z planes of the work-piece [8]. Therefore, the strength of ECAP resides in its versatility and ability to reproduce different microstructures and textures via numerous conventional processing methods such as rolling and drawing, just by changing the strain path [9]. Furthermore, it is found that the ECAP process yields a lamellar microstructure when the orientation of the billet is not changed after each pass and the development of combined ECAP routes involving orthogonal deformation paths contributes to achievement of smaller grains and a more equiaxed microstructure [10,11]. The advantage of this processing technique has been manifested by the improved properties of materials, including mechanical properties and physical properties [12]. Some promising improvement of strength in different materials, for example, copper, Al-alloys, pure Ti, Cu-based alloys, low-carbon steel, processed by ECAP has been achieved recently [13–17].

The austenitic stainless steel is one of the important structural materials and has many applications in industry mainly because of its excellent corrosion resistance [18–22]. However, its low yield strength is often a major drawback. Since severe plastic deformation (SPD) techniques such as ECAP or high-pressure

\* Corresponding authors. Tel.: +86 24 23971043.

E-mail addresses: shdwu@imr.ac.cn (S.D. Wu), zhfzhang@imr.ac.cn (Z.F. Zhang).

torsion (HPT) can effectively improve the yield strength of materials, it is reasonable to consider applying such a technique to austenitic stainless steel. Belyakov et al. [23] investigated initial grain size effect on the evolution of sub-microcrystalline structure during multiple compression of a 304 stainless steel at 600 °C. They found that the ultra-fine grains were developed as a result of a continuous increase in the misorientations between the subgrains evolved during deformation. In the samples with grain size smaller than 3.5  $\mu\text{m}$ , the fraction of strain-induced high-angle boundaries rapidly increases to more than 60% with a strain of about 1.5. However, their fraction does not exceed 20% at a strain of 1.5 in the sample with grain size of 15  $\mu\text{m}$ . Besides, they investigated the static restoration mechanisms operating during annealing in a 304 stainless steel at a strain-induced submicron grain microstructure [24]. Yapici et al. [25] studied the microstructure refinement and deformation twinning in 316L stainless steel subjected to ECAP. Recently, Huang et al. [26] successfully obtained bulk nanocrystalline grain structures in ultra-low carbon stainless steel by means of ECAP at room temperature. TEM investigations indicated that two types of nanostructures were formed: nanocrystalline strain-induced martensite with a mean grain size of 74 nm and nanocrystalline austenite with a size of 31 nm characterized by dense deformation twins. This result suggests that low stacking fault energy is exceptionally profitable for producing nanocrystalline materials by ECAP. Although there are some reports on the microstructure evolution of the ECAPed stainless steel, the corresponding mechanical properties of the ECAPed stainless steel with a relatively fine microstructure were not adequately explored.

On the other hand, as a work-piece is pressed through an ECAP die, it is generally accepted that the large shear deformation always occurs along the intersection plane between the entrance and exit channels. So, the intersection plane is just the shear deformation plane [27,28]. Based on the consideration above, some experiments were designed to investigate the influence of the shear plane on the mechanical properties of the materials subjected to the ECAP. Fang et al. [29] found that there are some streamline plane along the shear direction in the lateral surface ( $Y$  plane) of Al–0.63% Cu alloy after one or two passes. The streamline plane makes an angle of about 27° with respect to the longitudinal axis and the tensile fracture plane of the ECAPed specimen is approximately parallel to the streamline. Besides, the anisotropic compressive strength was clearly observed in the ECAPed pure iron by Han et al. [30], who attributed this anisotropy to the relatively weak resistance to shear deformation along such shear plane. This indicates that the ECAP shear plane along the flow line direction plays an important role in the deformation and fracture of those ECAPed materials.

In the present work, the compressive and tensile properties of AISI 304L stainless steel subjected to ECAP were systematically investigated in order to establish the relations among the number of ECAP passes, microstructure, mechanical properties and the deformation and fracture modes. Furthermore, the anisotropic compressive mechanical properties of the AISI 304L stainless steel were discussed for a better understanding of the ECAP mechanism.

## 2. Material and experimental procedure

The chemical composition of the investigated material (AISI 304L stainless steel) is given in Table 1. The sample subjected to ECAP was prepared from a rod of  $\varnothing$  8 mm diameter which was annealed at 1150 °C for 2 h. Processing by ECAP was performed under a plunge speed of 9–10 mm/s at 700 °C using a die with an angle  $\phi$  of 90° between the two channels, which yielded an effective strain of  $\sim 1$  for each pass. The stainless steel was ECAP-processed for one or four passes with route B<sub>C</sub> (90° sample clockwise rotation around the sample axis between the pass).

Firstly, the microstructures of the samples were observed by optical microscope (OM) and transmission electron microscope (TEM), respectively, on the transversal plane ( $X$  plane) and lateral plane ( $Y$  plane). For TEM observation, slices with a thickness of 0.5 mm were cut from transversal plane of the as-received and ECAPed rods, then manually thinned to 45  $\mu\text{m}$  and cut into disc with a diameter of 3 mm. Thin foils were made from these discs with a twin-jet polisher and a current of 90 mA used for an electrolyte of 10% perchloric acid at room temperature. The thinned discs were examined using a JEM 2000FXII TEM operating at 200 kV. The grain size was calculated and estimated by a combination of the linear intercept method and TEM observations. Secondly, the samples used for compressive experiments were machined from the as-received and ECAPed bars with three orientations (see Fig. 1). The angles between the compression axis and the extrusion direction are 0° (sample A), 45° (sample B) and 90° (sample C), respectively. All the compressive sam-

Table 1  
Chemical composition of the initial material AISI 304L

Element	C	Mn	Si	Cr	Ni	P	S
Concentration (%)	0.025	<0.5	0.36	18.75	10.96	0.068	0.005

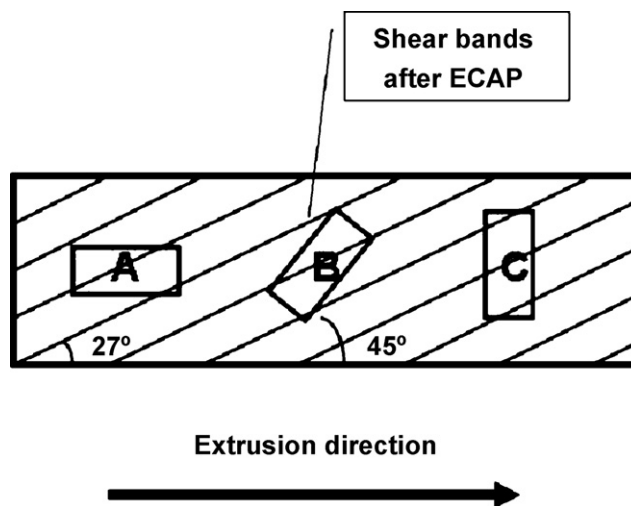


Fig. 1. Compressive sample orientations with respect to the ECAP billet geometry. The inclined lines indicate the shear flow plane from the one pass or four passes. The angles between extrusion direction and compression axis are equal to 0°, 45° and 90°, respectively.

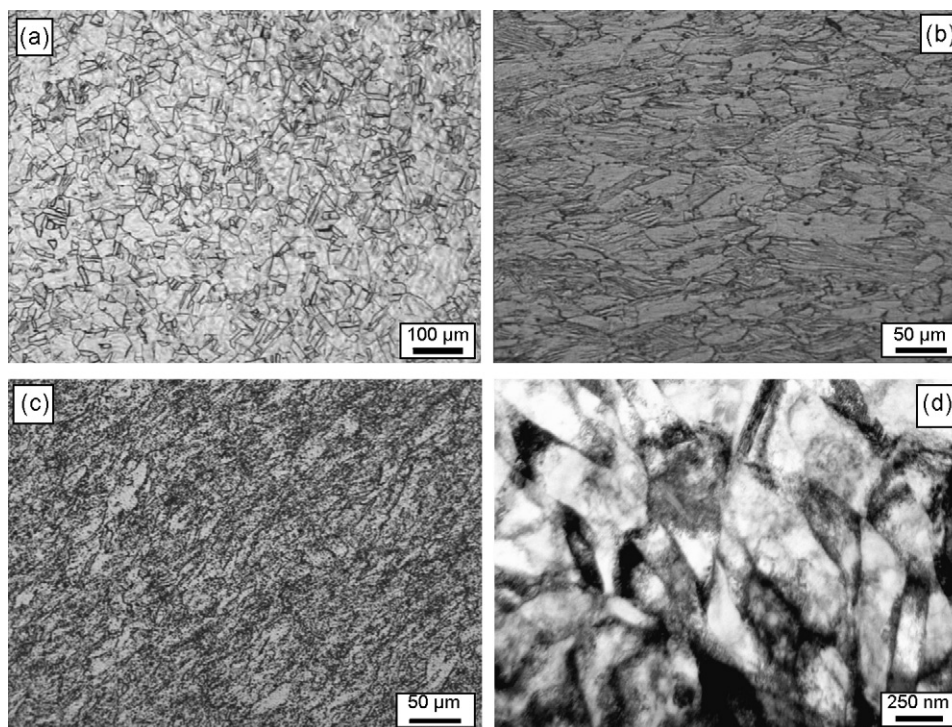


Fig. 2. Microstructures of AISI 304L stainless steel observed on  $X$  plane: (a) as-received; ECAPed for (b) one pass and (c) four passes observed by optical microscope; (d) four passes observed by TEM.

ples were rectangular block with a size of  $3\text{ mm} \times 3\text{ mm} \times 6\text{ mm}$ . Compressive tests were carried out at room temperature using an MTS 810 material testing system with a strain rate of  $10^{-4}\text{ s}^{-1}$ . Thirdly, the tensile specimens were cut from the as-received and ECAPed bars with the tensile axis parallel to the extrusion direction and had a dog-bone shape with a gauge section of  $1.5\text{ mm} \times 3\text{ mm} \times 15\text{ mm}$ . Tensile tests were performed at room temperature using MTS 858 Mini Bionix testing system with a strain rate of  $10^{-3}\text{ s}^{-1}$ . Then, the Vickers hardness was measured using a MVK-H3 Vickers microhardness tester. To make an exact measurement, the tests were performed with different loads of 100 g (as-received and one pass) and 200 g (four passes) for 10 s. Each specimen was measured for 15 times and the average value is as the measured hardness. A Cambridge S360 scanning electron microscope (SEM) or a LEO SUPERA 35 field emission SEM was employed to observe the deformation and fracture morphologies of the specimens after compressive and tensile tests.

### 3. Results and discussion

#### 3.1. Microstructures before and after ECAP

The initial microstructure of the as-received stainless steel is shown in Fig. 2a. It can be seen that the grains are approximately equiaxed and homogeneously distributed. The mean grain size, measured by the line intercept method, is about  $52\text{ }\mu\text{m}$ . Besides, there are some annealing twins with different orientations within the grains. Fig. 2b and c show the microstructures of the ECAPed samples for one pass and four passes observed on the cross-

section of the sample (i.e.  $X$  plane). After one pass, the grains were elongated along the vertical direction of cross-section and many slip bands appeared in most grains (Fig. 2b). After four passes, the grains were further refined, as shown in Fig. 2c. The TEM microstructure of the sample ECAP-processed for four passes shows that the large grains have been broken into small and homogeneous ones with size of about  $200\text{--}500\text{ nm}$  (see Fig. 2d).

From the results above, it can be seen that ECAP can effectively refine the microstructure of the AISI 304L stainless steel. On one hand, the grains are homogeneously distributed and refined into submicron size after ECAP processing. On the other hand, the grains were elongated on the  $Y$  plane after ECAP treatment for one pass, as shown in Fig. 3. The flow shear bands are parallel each other and make an angle of about  $27^\circ$  with respect to the extrusion direction, which is consistent with the previous results obtained in Al–Cu alloy and pure iron [29,30].

#### 3.2. Compressive properties

##### 3.2.1. Effect of ECAP on the strength and strain hardening rate

The compressive true stress–strain curves of the as-received and ECAPed samples (A, B and C) with different orientations are shown in Fig. 4. The detailed data about yield strength and strain hardening rate are listed in Table 2. For the as-received samples A, B and C, their strengths and strain hardening rates are almost identical (see Fig. 4a). This indicates that the yield strength and strain hardening rate of the as-received samples are independent of the orientations with respect to the load-

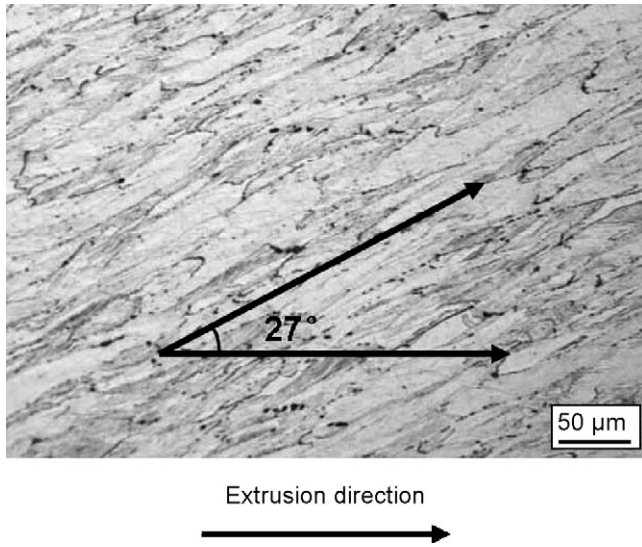


Fig. 3. Optical micrograph of shear bands observed on the Y plane of the ECAPed sample for one pass. The shear bands approximately make an angle of  $27^\circ$  with respect to the extrusion direction.

ing direction, showing an isotropic feature. After pressing for one pass, it is obvious that the yield strength of the samples has been significantly improved from  $\sim 200$  to  $\sim 800$  MPa, but displays a great anisotropy (see Fig. 4b). The strengths of the three samples that were ECAP-processed for one pass increase in the order B, C and A. However, after pressed for four passes, the samples A and C have almost the same strength and strain hardening rate even though they have different orientations with respect to the loading direction, as shown in Fig. 4c.

Fig. 5a and b shows the dependence of yield strength and strain hardening rate on the angle between the extrusion direction and loading axis. It can be seen that the yield strength of the as-received sample is independent of the orientations. However, an obvious anisotropy in the yield strength appears after one pass and this tendency becomes weak after four passes. This indicates that the ECAP can cause an obvious anisotropy in yield strength of the stainless steel. According to Fig. 4a–c, the linear strain hardening rate can be calculated by the following equation,

$$\frac{d\sigma}{d\varepsilon} = \frac{\Delta\sigma}{\Delta\varepsilon}. \quad (1)$$

The values  $\Delta\varepsilon$  and  $\Delta\sigma$  were measured from the straight segment of the stress–strain curves and the detailed data are listed in Table 2. It can be seen that the linear strain hardening rate is nearly independent of the sample orientations after one pass. It

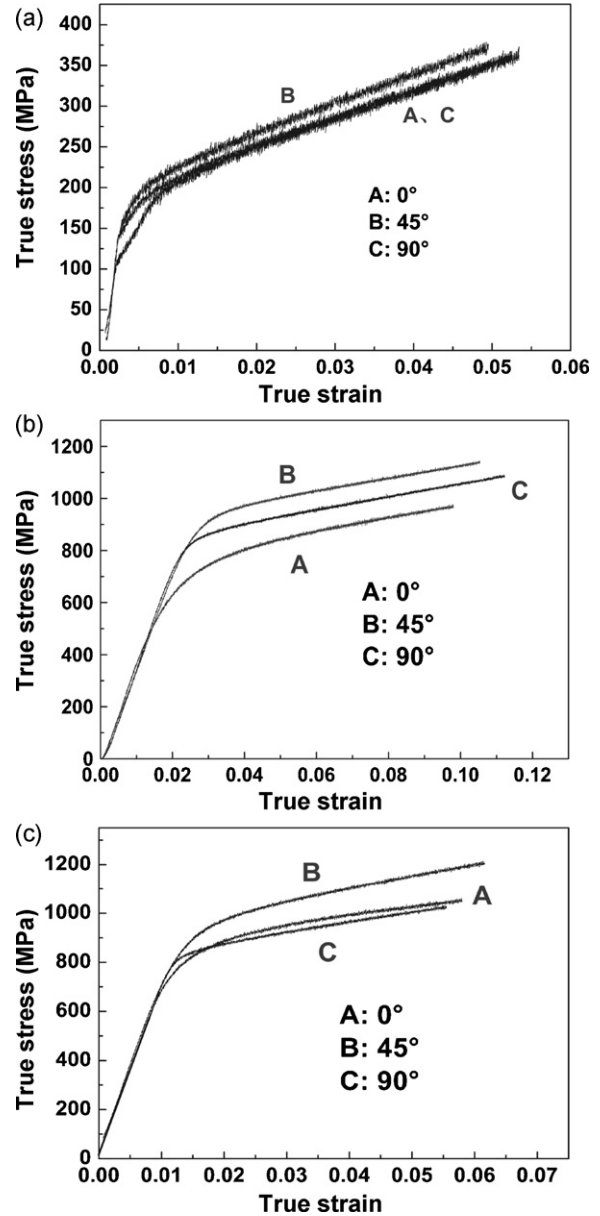


Fig. 4. Compressive stress–strain curves of the AISI 304L stainless steel samples with different orientations: (a) as-received, ECAPed for (b) one pass and (c) four passes.

is surprising that the strain hardening rate of the sample B is greatly higher than the samples A and C. It is suggested that the anisotropy in strain hardening rate become apparent at the fourth pass.

Table 2

The yield stress and strain hardening rate of the as-received and the ECAPed samples with different angles respect to the extrusion direction

	Processing condition								
	As-received			ECAP for one pass			ECAP for four passes		
	Angle $0^\circ$	Angle $45^\circ$	Angle $90^\circ$	Angle $0^\circ$	Angle $45^\circ$	Angle $90^\circ$	Angle $0^\circ$	Angle $45^\circ$	Angle $90^\circ$
Yield stress (MPa)	150	199	176	652	877	850	768	881	832
$d\sigma/d\varepsilon$ (GPa)	3.50	3.70	3.50	5.20	5.29	5.12	3.90	5.80	4.30

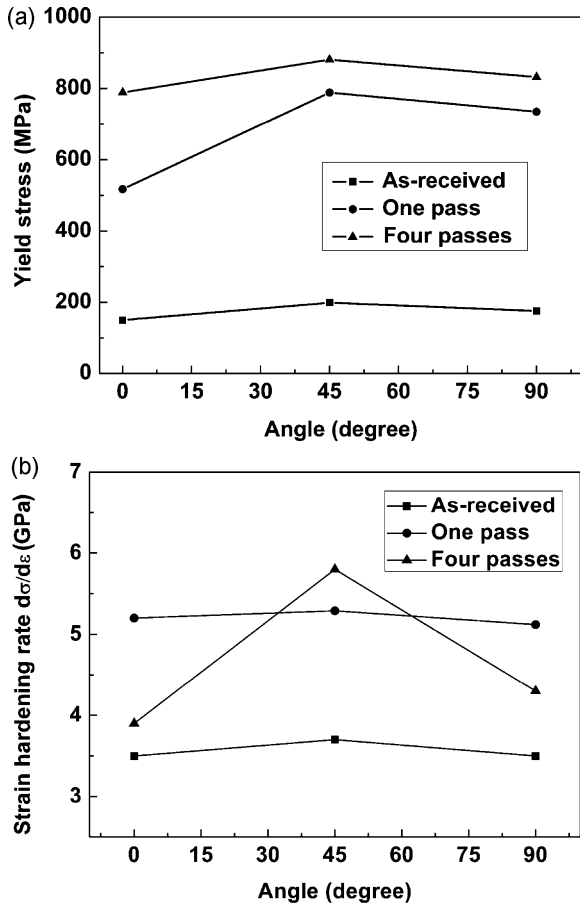


Fig. 5. Dependence of (a) yield stress and (b) strain hardening rate on the number of ECAP passes and the angle between the extrusion direction and the compression axis.

### 3.2.2. Compressive deformation morphologies

Fig. 6a shows the SEM micrographs of the as-received AISI 304L stainless steel after compressive tests. It can be seen that there are many slip bands within the different grains. The slip

bands are parallel to each other inside the grains and some double-slip bands were activated locally. Fig. 6b–d shows the SEM micrographs of the ECAPed AISI 304L stainless steel after compressive experiment. After four passes, there exists the streamline feature in the lateral surface of the compressive samples. The streamline planes make different angles of about  $25^\circ$ ,  $18^\circ$  and  $67^\circ$  with respect to the compressive direction, respectively, for the samples A, B and C. The orientations of the streamline planes are almost consistent with the direction of the shear planes of the ECAPed samples [29,30]. This indicates that the shear planes formed by ECAP are approximately parallel to the shear bands during compression deformation.

### 3.2.3. Effect of orientations on the compressive strength

To explain the anisotropy of yield and flow stresses, one can consider the formation of the shear planes subjected to ECAP processing. Fig. 3 shows the optical microstructure of the lateral plane ( $Y$  plane) after one-pass ECAP. During pressing, the grains were elongated along the direction at an angle of about  $27^\circ$  with respect to the extrusion direction [29,30]. Meanwhile, the elongated grain boundaries formed many parallel shear lines on the lateral surface, which are considered as relatively weak planes to resist shear deformation [30]. So, those shear planes should be easily activated when the specimen is subjected to a compressive load. According to the sample orientations in Fig. 1a–c, the shear planes will make approximate angles of  $27^\circ$ ,  $18^\circ$  and  $63^\circ$  with respect to the compressive direction, respectively, for the samples A ( $0^\circ$ ), B ( $45^\circ$ ) and C ( $90^\circ$ ) (see Fig. 7a–c). Therefore, the shear stress  $\tau_s$  on the shear plane can be expressed as

$$\tau_s = \sigma_c \sin\theta \cos\theta, \quad (2)$$

where  $\sigma_c$  is the compressive stress and  $\theta$  is the angle between the shear plane and the loading direction, as illustrated in Fig. 8. For samples A, B and C, the angles  $\theta$  are approximately equal to  $27^\circ$ ,  $18^\circ$  and  $63^\circ$ , respectively. According to Eq. (2), the compressive

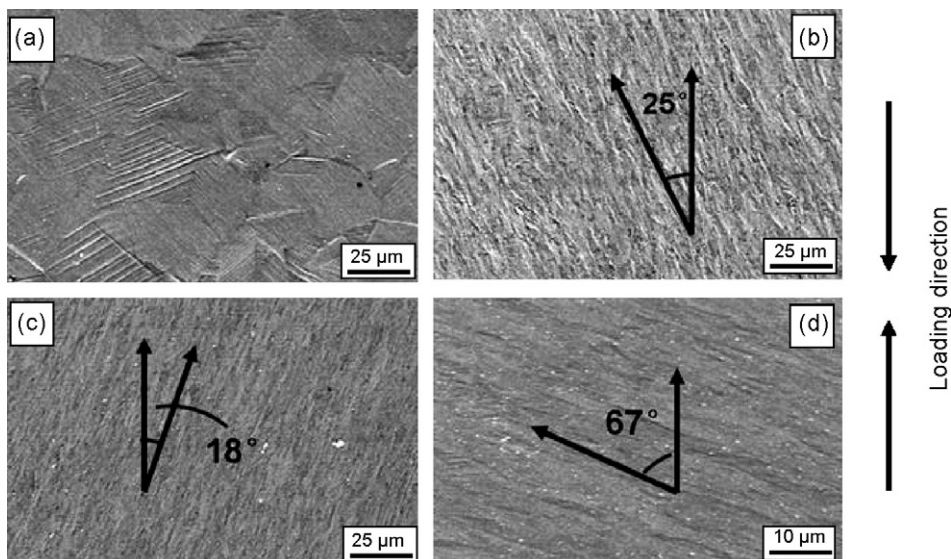


Fig. 6. SEM micrograph of samples after compression: (a) as-received and ECAPed for four passes, (b) sample A, (c) sample B and (d) sample C.

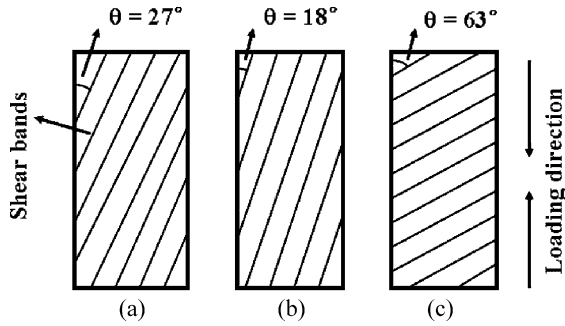


Fig. 7. Illustration of the shear band distribution in the samples A, B and C with an interaction angle of  $27^\circ$ ,  $18^\circ$ ,  $63^\circ$ , respectively. Here,  $\theta$  is the angle between the shear bands and the loading direction and  $\phi$  is the angle between the compression axis and the extrusion direction. (a) Sample A ( $\phi = 0^\circ$ ), sample B ( $\phi = 45^\circ$ ) and sample C ( $\phi = 90^\circ$ ).

strength can be expressed as

$$\sigma_c = \frac{\tau_s}{\sin\theta \cos\theta}. \quad (3)$$

Han et al. [30] have proved that the shear plane is a weak plane resisting shear deformation in the ECAPed pure iron. If considering the critical shear strength  $\tau_s$  is nearly the same, the compressive strength  $\sigma_c$  should be a function of the angle  $\theta$  between the shear plane and the loading direction. Substituting  $\theta_A = 27^\circ$ ,  $\theta_B = 18^\circ$  and  $\theta_C = 63^\circ$  into Eq. (3), the three compressive strengths should be equal to

$$\sigma_c^A = \frac{\tau_s}{\sin 27^\circ \cos 27^\circ} = 2.4\tau_s \quad (4a)$$

$$\sigma_c^B = \frac{\tau_s}{\sin 18^\circ \cos 18^\circ} = 3.4\tau_s \quad (4b)$$

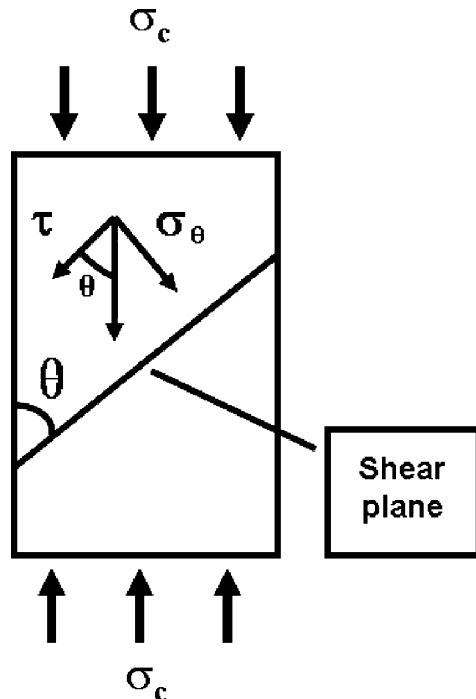


Fig. 8. Illustration of the normal and shear stresses on the shear plane of the AISI 304L stainless steel sample ECAPed for one pass under compressive test.

$$\sigma_c^C = \frac{\tau_s}{|\sin 63^\circ \cos 63^\circ|} = 2.4\tau_s. \quad (4c)$$

Therefore, one can get

$$\sigma_c^B > \sigma_c^A = \sigma_c^C. \quad (5)$$

This is approximately consistent with the compressive stress–strain curves in Fig. 4a–c. However, considering the pressure effect of shear deformation [31,32], the compressive strength of the sample C should be higher than that of the sample A because  $\theta_C = 63^\circ$  is larger than  $\theta_A = 27^\circ$ .

After four ECAP-passes, the compressive strength of the sample C is quite close to that of the sample A, indicating that the strength parallel to the extrusion direction is approximately equal to that vertical to the extrusion direction. However, the sample B displays a much higher compressive strength than of the samples A and C. Thus, it can be concluded that the anisotropy in compressive strength still exists in the sample ECAPed for four passes (see Fig. 4c).

### 3.3. Tensile properties

#### 3.3.1. Effect of ECAP on tensile properties

The tensile true stress–strain curves of the AISI 304L stainless steel are shown in Fig. 9. It can be seen that the annealed stainless steel yielded at a very low stress of about 168 MPa, but displayed a strong strain hardening behavior and failed at a fracture stress of 556 MPa. After one ECAP-pass, its yield strength was greatly improved to about 710 MPa, however, its strain hardening rate became relatively low. When the material was pressed for four passes, its yield strength was further increased to about 1121 MPa and displayed little strain hardening behavior. The great improvement in yield strength can be attributed to the grain refinement (see Fig. 2b–d) and the increase in the dislocation density [33–36]. The variations of yield and fracture strengths are clearly shown in Fig. 10a. With the increase in the strength of the ECAPed samples, its elongation obviously decreases from 61 to 12%, as shown in Fig. 10b. This tendency related to strength and elongation is consistent with many other ECAPed metals or alloys [37–41].

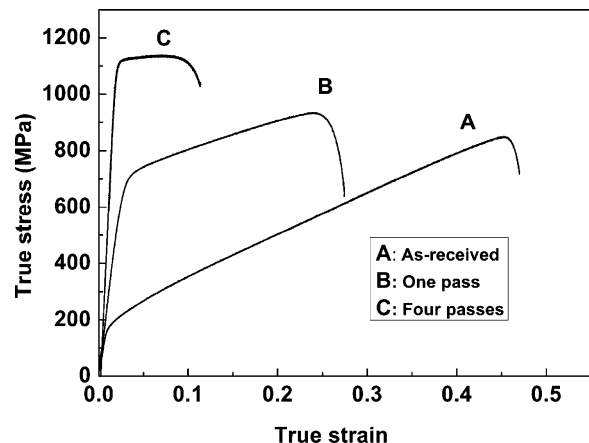


Fig. 9. Tensile true stress–strain curves of the AISI 304L stainless steel subjected to ECAP for 0, 1 and 4 passes, respectively.

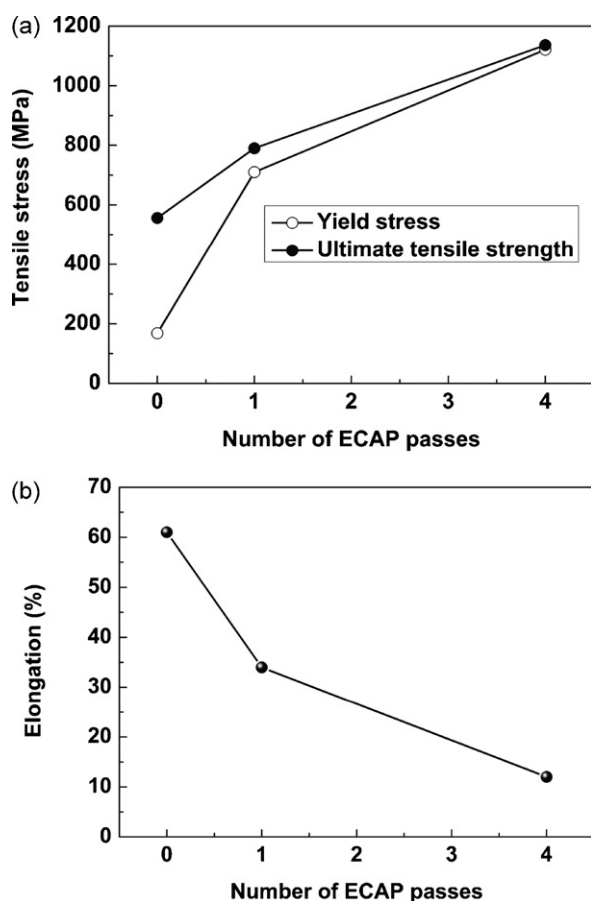


Fig. 10. Dependence of (a) yield strength, ultimate tensile strength and (b) elongation on the number of ECAP passes of the AISI 304L stainless steel.

### 3.3.2. Tension–compression asymmetry

Except for the variation of strength and elongation, there exists a significant tension–compression asymmetry in the ECAPed samples parallel to the extrusion direction, and some data are listed in Table 3. The asymmetry of the yield strength is distinct after four passes (see Fig. 11a). On the other hand, for the strain hardening rate, there is a decreasing tendency after one pass (see Fig. 11b). The similar tension–compression asymmetry was also observed in the Fe–10Cu [42], submicron-grained Al [43], 316L stainless steel [25] and Al–Fe–Cr–Ti alloy [44]. Yapici et al. [25] suggested that texture and directional internal stress are two possible reasons for this behavior and proved that directional internal stress is the main reason for the tension–compression asymmetry in the submicron-grained 316L stainless steel.

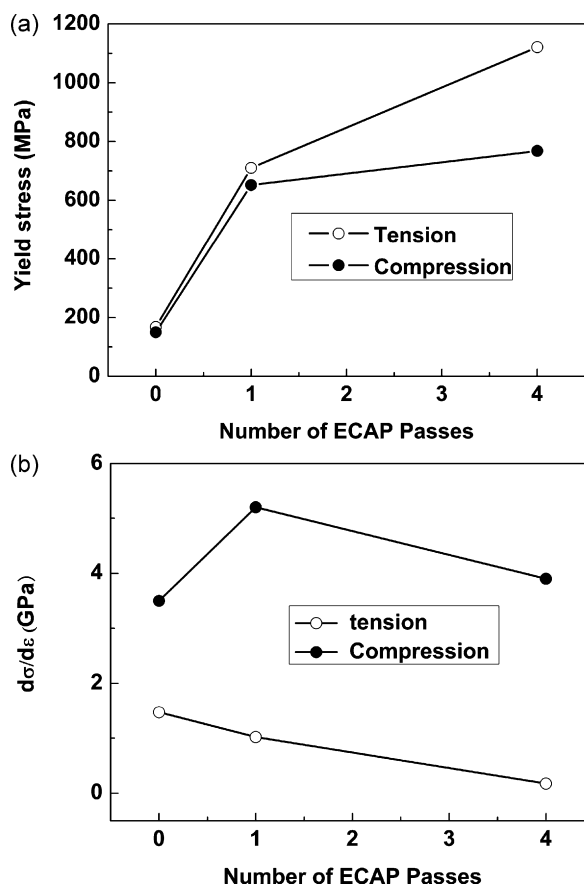


Fig. 11. Comparison of (a) yield stress and (b) strain hardening rate of the AISI 304L stainless steel under compression and tension loads.

However, Luo et al. [44] eliminated the extrinsic factors such as processing defects and residual stresses and proved that the tension–compression asymmetry is an intrinsic property of the nanocrystalline Al–Fe–Cr–Ti alloy. They indicated that this asymmetry resulted from the interplay of limited dislocation accumulation in nanograins, the associated rapid stress built up within the grains, at the grain boundaries, and at the interfaces between fcc-Al grains and intermetallic particles. Moreover, Cheng et al. [45] proposed a deformation mechanism for FCC metals with grain size ranging from nanometer to micrometer scale based upon classical dislocation theory. They suggested that the strength-limiting mechanism in metals with submicron-grained (SMG) structure was dislocation bow-out from grain boundary sources, and that the yield strength asymmetry arose from the pressure dependence of the dislocation self-energy during bow-out. Under a uniaxial stress  $\sigma$ , the value of the applied

Table 3

Summary of the microstructure observation and results of the mechanical experiments conducted at room temperature

Processing condition	Tension				Compression (specimen A)		Hardness (GPa)
	$\sigma_y$ (MPa)	UTS (MPa)	$\varepsilon$ (%)	$d\sigma/d\varepsilon$ (GPa)	$\sigma_y$ (MPa)	$d\sigma/d\varepsilon$ (GPa)	
As-received	168	556	61	1.473	150	3.5	1.33
ECAP, one pass	710	790	34	1.020	652	5.2	2.21
ECAP, four passes	1121	1136	12	0.175	768	3.9	3.02

Note: ( $\sigma_y$ ) yield strength; (UTS) ultimate tensile strength; ( $\varepsilon$ ) tensile fracture strain; ( $d\sigma/d\varepsilon$ ) strain hardening rate.

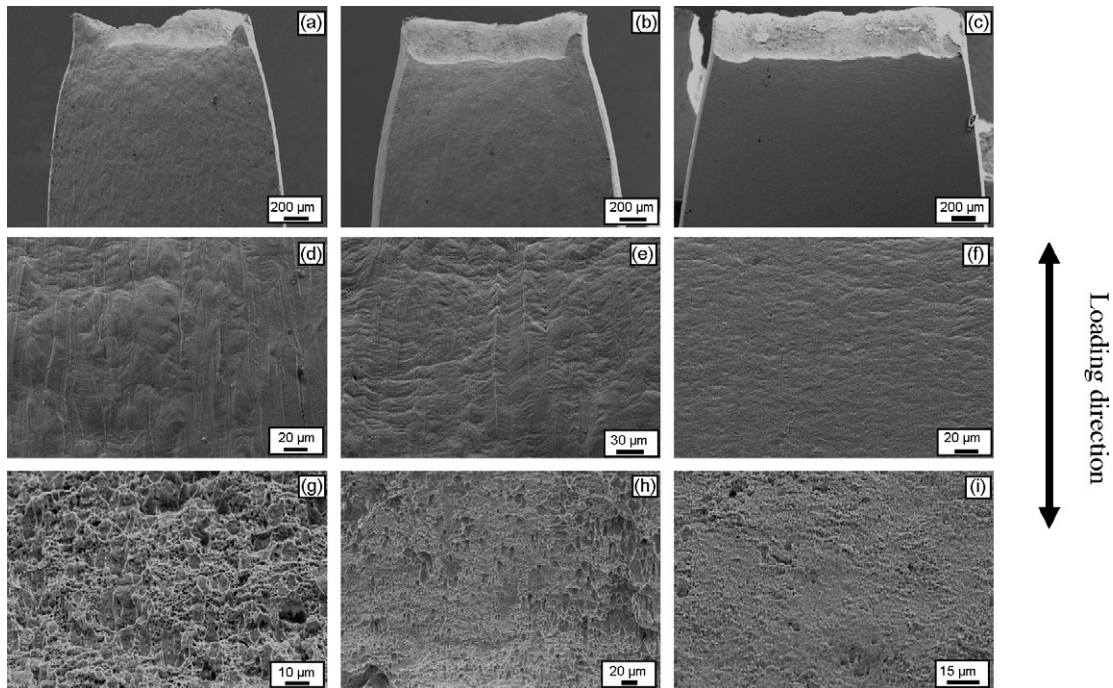


Fig. 12. Different necking degree of the tensile fractography: (a) as-received, ECAPed for (b) one pass and (c) four passes and slip bands; shear bands on the lateral surfaces, (d) as-received, ECAPed for (e) one pass and (f) four passes; different dimple features on the tensile fractography, (g) as-received, ECAPed for (h) one pass and (i) four passes.

hydrostatic pressure is  $+\sigma/3$  in compression and  $-\sigma/3$  in tension. It turns out that this has a large effect on the stress necessary to activate the grain boundary dislocation source when the source length is small.

### 3.3.3. Tensile deformation and fracture morphologies

Fig. 12 shows the SEM micrographs for the deformation and fracture morphologies of the as-received and ECAPed AISI 304L stainless steel after tensile tests. The as-received specimen shows an obvious necking feature before failure and the shear lip was formed around the fracture surface, as shown in Fig. 12a. The one-pass ECAPed specimen also displays necking (see Fig. 12b). After pressed for four passes, the specimen shows little necking and the fracture surface is almost flat (see Fig. 12c).

For the as-received specimen, the grains were elongated along the tensile axis (see Fig. 12d), indicating a high tensile plasticity. Within the elongated grains, there are some slip bands perpendicular to the fracture plane, which results from the necking deformation (see Fig. 12d). After ECAP for one pass, on the lateral surface, the longitudinal shear bands which caused by the necking deformation become weak because of the decrease in necking degree. However, the shear bands on the lateral surface become exiguous when the specimen was subjected to four passes of ECAP. This indicates that the specimen displays a weak necking on the lateral surface (see Fig. 12e and f). At high magnification, it is clearly seen that the fracture surface of the as-received specimen contains many deep dimples homogeneously distributed like honeycombs (see Fig. 12g). After ECAP for one pass, the dimples become smaller and shallower (see Fig. 12b). Finally, the small dimples only appear in local areas and there

are many smooth areas distributed on the fracture surface of the specimen ECAPed for four passes (see Fig. 12h and i).

From the results above, it can be concluded that the as-received stainless steel has a good ductility and displays typical features of ductile fracture. But with increasing the number of the ECAP passes, the fracture mode is changed from ductile to brittle which provides an evidence for the decrease in the ductility of the ECAPed AISI 304L stainless steel.

### 3.4. Relation between hardness and strength

From Fig. 13, it can be seen that the hardness tends to be enhanced with increasing the numbers of ECAP passes, and the

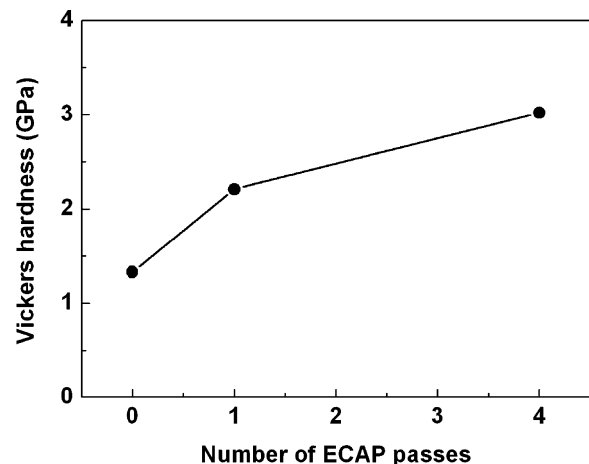


Fig. 13. Dependence of Vickers hardness on the number of ECAP passes of the AISI 304L stainless steel.

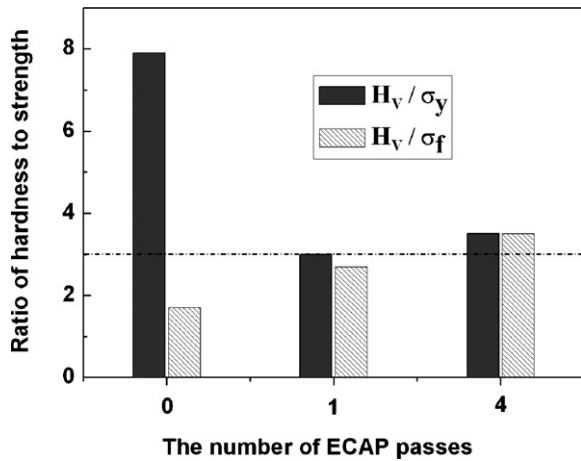


Fig. 14. Relationship between  $H_V$  and  $\sigma_y(\sigma_f)$  for as-received and ECAPed AISI 304L stainless steel samples.

data are listed in Table 3. Meanwhile, it is well known that there is an empirical relationship, i.e.  $H_V/3 \approx \sigma_f$  [46], between the strength  $\sigma_f$  and Vickers hardness  $H_V$ . Fig. 14 shows the dependence of  $H_V/\sigma_y$  and  $H_V/\sigma_f$  on the number of ECAP passes for the stainless steel. It can be seen that for the as-received specimen, the ratios of  $H_V/\sigma_y$  and  $H_V/\sigma_f$  are equal to 7.9 and 1.7, respectively, and thus obviously different from the constant 3. However, the specimens that were ECAP-processed for one and four passes have almost the same ratio of  $H_V/\sigma_y$  or  $H_V/\sigma_f$ , which are quite close to the constant 3. This indicates that the hardness of the ECAPed specimens for one and four passes approximately follows the empirical relationship of  $H_V/3 \approx \sigma_f$ .

Since the hardness of the as-received specimen follows the relationship  $\sigma_y < H_V/3 < \sigma_f$  (see Fig. 14), for simplicity, it is assumed that the hardness  $H_V$  of such materials can be expressed as a function of the yield strength  $\sigma_y$  and the fracture strength  $\sigma_f$ , i.e.

$$\frac{H_V}{3} = x\sigma_y + (1-x)\sigma_f, \quad (6)$$

where  $x$  represents the contribution of yield strength  $\sigma_y$  to the hardness and  $(1-x)$  represents the contribution of the fracture strength  $\sigma_f$  to the hardness [47]. In the present study, the value of  $x$  for the as-received specimen is 0.34, as calculated by Eq. (6) and the data in Table 3. After ECAP of the stainless steel, due to the severe strain hardening, both yield and fracture strengths are enhanced, leading to a higher hardness too. Finally, the yield strength tends to have the same value as the fracture strength; accordingly, the ratio  $H_V/\sigma_y$  or  $H_V/\sigma_f$  of strength to hardness is also inclined to a constant value of 3, as shown in Fig. 14.

#### 4. Conclusions

From the experimental results above, it can be concluded that the ECAP processing has an important influence on the microstructure, mechanical properties and tensile fracture modes of AISI 304L stainless steel. The following conclusions can be drawn.

1. Grains of the AISI 304L stainless steel were refined to the submicron size after ECAPed for four passes and were elongated along the angle of  $27^\circ$  with respect to the extrusion direction on the  $Y$  plane of the one-pass sample which formed the shear plane in the compressive samples. Furthermore, the shear bands formed in the compressive test prove that the compressive deformation is mainly along the direction of these shear planes.
2. ECAP can obviously cause the anisotropy in mechanical properties especially under compressive test. The anisotropy in yield strength is significantly increased after one ECAP pass. However, it becomes weak after four passes. Its strain hardening rate is also increased after one pass, compared to four passes. The shear planes formed after ECAP processing seem to be the relatively weak planes, leading to the anisotropy in compressive yield strength.
3. ECAP can effectively increase the Vickers hardness, tensile yield and fracture strengths, but decrease the elongation and the strain hardening rate of the AISI 304L stainless steel. The fracture mode was changed from the ductile to the brittle after the ECAP treatment.
4. The Vickers hardness is increased with increasing the number of ECAP passes and the relation between hardness and strength is changed by the ECAP treatment. The Vickers hardness of the as-received specimen follows the relation of  $\sigma_y < H_V/3 < \sigma_f$ ; however, after ECAP treatment, the hardness approximately follows the empirical relation of  $H_V/3 \approx \sigma_f$ .

#### Acknowledgements

The authors would like to thank Gao W, Su HH, Wen JL, Yao G, for the assistance in the mechanical tests, SEM observations and stimulating discussions on the manuscript. This work was supported by ‘‘Hundred of Talents Project’’ of the Chinese Academy of Sciences and the National Natural Science Foundation of China (NSFC) under Grant No. 50571102. Financial support by the National Outstanding Young Scientist Foundation for Z.F. Zhang under Grant No. 50625103 is also acknowledged.

#### References

- [1] J. Kim, I.T. Kim, D.H. Shin, Scripta Mater. 44 (2001) 1503.
- [2] Y. Iwahashi, M. Horita, M. Nemoto, Metall. Mater. Trans. A 29 (1998) 2245.
- [3] R.Z. Valiev, I.V. Alexandrov, Nanostruct. Mater. 12 (1999) 35.
- [4] C.X. Huang, K. Wang, S.D. Wu, Z.F. Zhang, G.Y. Li, S.X. Li, Acta Mater. 54 (2006) 655.
- [5] V.M. Segal, V.I. Reznikov, A.E. Drobyshevskiy, V.I. Kopylov, Russian Metall. 1 (1981) 99.
- [6] Y. Iwahashi, Z. Horita, M. Nemoto, T.G. Langdon, Acta Mater. 46 (1998) 3317.
- [7] V.M. Segal, Mater. Sci. Eng. A 197 (1995) 157.
- [8] M. Furukawa, Y. Iwahashi, Z. Horita, M. Nemoto, Mater. Sci. Eng. A 257 (1998) 3.
- [9] M. Haouaoui, I. Karaman, H.J. Maier, Acta Mater. 54 (2006) 5477.
- [10] O.V. Mishin, D.J. Jensen, N. Hansen, Mater. Sci. Eng. A 342 (2003) 320.
- [11] V.V. Stolyarov, Y.T. Zhu, I.V. Alexandrov, T.C. Lowe, R.Z. Valiev, Mater. Sci. Eng. A 299 (2001) 59.
- [12] S.H. Lee, H. Utsunomiya, T. Sakai, Mater. Trans. 45 (2004) 2177.

- [13] F.D. Torre, R. Lapovok, J. Sandlin, P.F. Thomson, C.H.J. Davies, E.V. Pereloma, *Acta Mater.* 52 (2004) 4819.
- [14] Z.G. Zhang, S. Hosoda, I.S. Kim, Y. Watanabe, *Mater. Sci. Eng. A* 425 (2006) 55.
- [15] V.V. Stolyarov, Y.T. Zhu, G.I. Raab, A.I. Zharikov, R.Z. Valiev, *Mater. Sci. Eng. A* 385 (2004) 309.
- [16] A. Vinogradov, V.Y. Suzuki, K. Kitagawa, V. Kopylov, *Acta Mater.* 50 (2002) 1639.
- [17] D.H. Shin, C.W. Seo, J. Kim, K.T. Park, W.Y. Choo, *Scripta Mater.* 42 (2000) 695.
- [18] J.W. Simmons, *Mater. Sci. Eng. A* 207 (1996) 159.
- [19] V. Tsakiris, D.V. Edmonds, *Mater. Sci. Eng. A* 273 (1999) 430.
- [20] I. Karaman, H. Schitoglu, H.J. Maier, Y.I. Chumlyakov, *Acta Mater.* 49 (2001) 3919.
- [21] I. Karaman, H. Sehitoglu, Y.I. Chumlyakov, H.J. Maier, *JOM* 54 (2002) 31.
- [22] R.L. Peng, M. Oden, Y.D. Wang, S. Johansson, *Mater. Sci. Eng. A* 334 (2002) 215.
- [23] A. Belyakov, K. Tsuzaki, H. Miura, T. Sakai, *Acta Mater.* 51 (2003) 847–861.
- [24] A. Belyakov, T. Sakai, H. Miura, R. Kaibyshev, K. Tsuzaki, *Acta Mater.* 50 (2002) 1547–1557.
- [25] G.G. Yapici, I. Karaman, Z.P. Luo, H.J. Maier, Y.I. Chumlyakov, *J. Mater. Res.* 19 (2004) 2268.
- [26] C.X. Huang, Y.L. Gao, G. Yang, S.D. Wu, G.Y. Li, S.X. Li, *J. Mater. Res.* 21 (2006) 1687.
- [27] V.M. Segal, *Mater. Sci. Eng. A* 197 (2002) 157.
- [28] S.R. Agnew, J.A. Horton, T.M. Lillo, D.W. Brown, *Scripta Mater.* 50 (2004) 377.
- [29] D.R. Fang, Z.F. Zhang, S.D. Wu, C.X. Huang, H. Zhang, N.Q. Zhao, J.J. Li, *Mater. Sci. Eng. A* 426 (2006) 305.
- [30] W.Z. Han, Z.F. Zhang, S.D. Wu, S.X. Li, Y.D. Wang, *Philos. Mag. Lett.* 86 (2006) 435.
- [31] Z.F. Zhang, J. Eckert, L. Schultz, *Acta Mater.* 51 (2003) 1167.
- [32] Z.F. Zhang, G. He, J. Eckert, L. Schultz, *Phys. Rev. Lett.* 91 (2003) 045505.
- [33] T.C. Hufnagel, P. El-Deiry, R.P. Vinci, *Scripta Mater.* 43 (2000) 1071.
- [34] S.C. Baik, Y. Estrin, H.S. Kim, R.J. Hellmig, *Mater. Sci. Eng. A* 351 (2003) 86–97.
- [35] V.V. Stolyarov, Y.T. Zhu, I.V. Alexandrov, T.C. Lowe, R.Z. Valiev, *Mater. Sci. Eng. A* 343 (2003) 43–45.
- [36] Z.C. Wang, P.B. Prangnell, *Mater. Sci. Eng. A* 328 (2002) 87–97.
- [37] G. Purcek, *J. Mater. Process. Technol.* 169 (2005) 242–248.
- [38] A. Azushima, K. Aoki, *Mater. Sci. Eng. A* 337 (2002) 45–49.
- [39] T.C. Chang, J.Y. Wang, C.L. Chu, S. Lee, *Mater. Lett.*, 2007, in press.
- [40] L.J. Chen, C.Y. Ma, G.M. Stoica, P.K. Liaw, C. Xu, T.G. Langdon, *Mater. Sci. Eng. A* 410–411 (2005) 472–475.
- [41] H.B. Geng, S.B. Kang, B.K. Min, *Mater. Sci. Eng. A* 373 (2004) 229–238.
- [42] J.E. Carsley, A. Fisher, W.W. Milligan, E.C. Aifantis, *Metall. Mater. Trans. A* 29 (1998) 2261.
- [43] C.Y. Yu, P.L. Sun, P.W. Kao, C.P. Chang, *Scripta Mater.* 52 (2005) 359.
- [44] H. Luo, L. Shaw, L.C. Zhang, D. Miracle, *Mater. Sci. Eng. A* 409 (2005) 249–256.
- [45] S. Cheng, J.A. Spencer, W.W. Milligan, *Acta Mater.* 51 (2003) 4505.
- [46] H.S. Chen, *Rep. Prog. Phys.* 43 (1980) 533.
- [47] X.F. Pan, H. Zhang, Z.F. Zhang, G. He, M. Stoica, J. Eckert, *J. Mater. Res.* 20 (2005) 2632.